

Rayleigh waves from correlation of seismic noise in Great Island of Tierra del Fuego, Argentina: Constraints on upper crustal structure

Carolina Buffoni ^{a,*}, Martin Schimmel ^b, Nora Cristina Sabbione ^a, María Laura Rosa ^a, Gerardo Connon ^{c,d}

^a Faculty of Astronomical and Geophysical Sciences, National University of La Plata, Paseo Del Bosque S/n B1900F WA, Argentina

^b Institute of Earth Sciences Jaume Almera – CSIC, Lluís Solé Sabarís S/n; Barcelona, E-08028, Spain

^c Astronomical Station of Río Grande (EARG), Ruta C y Acceso Aeropuerto, 9420EAR, Río Grande, Argentina

^d National Scientific and Technical Research Council (CONICET), Av. Rivadavia 1917 C1033AAJ, Autonomous City of Buenos Aires, Argentina

ARTICLE INFO

Article history:

Received 13 July 2017

Accepted 28 November 2017

Available online 7 December 2017

Keywords:

Ambient seismic noise cross-correlation

Rayleigh wave dispersion

Upper crust

Tierra del Fuego

ABSTRACT

In this study, the ambient seismic noise cross-correlation technique is applied to estimate the upper structure of the crust beneath Great Island of Tierra del Fuego (TdF), Argentina, by the analysis of short-period Rayleigh wave group velocities. The island, situated in the southernmost South America, is a key area of investigation among the interaction between the South American and Scotia plates and is considered as a very seismically active one. Through cross-correlating the vertical components of ambient seismic noise registered at four broadband stations in TdF, we were able to extract Rayleigh waves which were used to estimate group velocities in the period band of 2.5–16 s using a time-frequency analysis. Although ambient noise sources are distributed inhomogeneously, robust empirical Green's functions could be recovered from the cross-correlation of 12 months of ambient noise. The observed group velocities were inverted considering a non-linear iterative damped least-squares inversion procedure and several 1-D shear wave velocity models of the upper crust were obtained. According to the inversion results, the S-wave velocity ranges between 1.75 and 3.7 km/s in the first 10 km of crust, depending on the pair of stations considered. These results are in agreement to the major known surface and sub-surface geological and tectonic features known in the area. This study represents the first ambient seismic noise analysis in TdF in order to constraint the upper crust beneath this region. It can also be considered as a successful feasibility study for future analyses with a denser station deployment for a more detailed imaging of structure.

© 2017 Institute of Seismology, China Earthquake Administration, etc. Production and hosting by Elsevier B.V. on behalf of KeAi Communications Co., Ltd. This is an open access article under the CC BY-NC-ND license (<http://creativecommons.org/licenses/by-nc-nd/4.0/>).

1. Introduction

The Great Island of TdF (Tierra del Fuego), southernmost South America, is transversed by a transform tectonic boundary between the South American and Scotia plates [1,2]. This boundary is characterized by a left-lateral strike slip regime represented by the

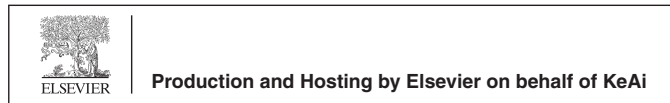
MFFS (Magallanes-Fagnano Fault System). The main fault of the MFFS, named the MFF (Magallanes-Fagnano Fault), runs from the western part of north Scotia ridge towards the Chile trench at about 50°S [3,4] and splits the island into two continental blocks (Fig. 1). Recent geodetic studies indicate that the movement in connection with the geodynamic process along the MFF is 5.9 ± 0.2 mm/year [5].

The present geological and tectonic environment of TdF is the result of the interaction between the South American, Scotia and Antarctic plates that involved the evolution of southernmost South America associated with the Andean orogenic cycle during the Mesozoic–Cenozoic. This evolution can be summarized by three tectonic episodes: an extensive regime (Late Jurassic– Early Cretaceous), a compression period (Cretaceous–Paleocene) and finally a strike-slip movement since the Oligocene [6]. The recent tectonic evolution of South America is associated with the geodynamic of

* Corresponding author. Fax: +54 221 4236591.

E-mail address: cbuffoni@fcaglp.unlp.edu.ar (C. Buffoni).

Peer review under responsibility of Institute of Seismology, China Earthquake Administration.



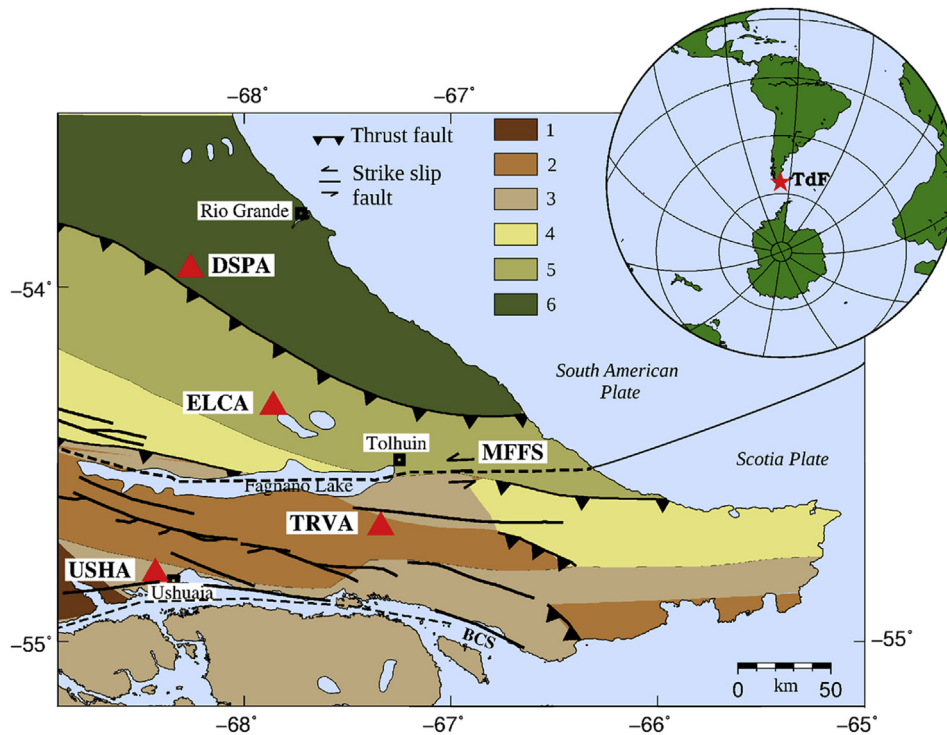


Fig. 1. Simplified geologic map of TdF adapted from Tassone et al. [8]. BCS, Beagle Channel fault system, MFFS, Magallanes-Fagnano Fault System. 1. Basement (Paleozoic–Jurassic), 2. Rhyolites, basalts, conglomerates, tuff and turbidites from Upper Jurassic (Lemaire Formation), 3. Lower Cretacic deposits (Yaghan and Beauvoir Formations), 4. Upper Cretacic deposits, 5. Deformed Tertiary deposits, 6. Undeformed Tertiary deposits. DSPA, ELCA, TRVA and USHA are the seismic stations used in this study. Rio Grande, Tolhuin and Ushuaia are the major cities. The different geologic units were determined by several authors [2,9–11].

the Scotia plate that moved continental fragments more than 1000 km away from TdF [7].

The MFFS controls the present-day tectonic setting in this area [12]. Geological and geomorphological evidences indicate that the MFF is parallel to the 105 km long Fagnano Lake [13]. The region situated to the south of the lake belongs to the Scotia plate that moves to the east. Geologically, this area is characterized by the Fuegian Cordillera composed by a Paleozoic basement and above this volcanic rocks that correspond to Middle to Upper Jurassic. These rocks are covered by Upper Cretacic and Tertiary deposits. Tectonically, the southern part of TdF presents morphological evidence of Quaternary activity related to the strike-slip regime. The area situated to the north of Fagnano Lake belongs to the South American plate that moves to the west and presents a geological stable extra-andean environment. This region is affected by a tectonic period of extension associated with normal faults to the east of the Magallanes Strait [6]. Other sub-parallel secondary faults that belong to the MFFS are: the Beagle Channel, the Deseado, the Lasifashaj, the Carbajal and the Rio Turbio faults [6,13]. Some of these are associated with normal faults dipping to N in the southern part of TdF. Furthermore, several normal faults with NO-SW strike and dipping to NE and SO were identified in the central and northern part of the island [6].

Since the 90s, a local seismic network started to register seismic movements associated with the MFFS. The seismicity in TdF is characterized by low magnitude events [12,14–17], regardless that this area is considered as a very seismically active one. The historical earthquake records include a magnitude 7.0 event in 1879 [18], several earthquakes of magnitude >6 during 1930 and 1944 and two important events on 1949 December 17 of magnitude 7.5 and 7.8 [19].

At present little information about the crustal structure of TdF is available. Some authors estimated crustal thickness ranging from

29 to 36 km near our study area through seismic refraction profiles [20], regional seismograms inversion [21] and receiver function and surface wave analyses [22]. In this study, we present new constraints on upper crustal structure beneath the Argentinian part of TdF considering the ambient seismic noise registered at 4 broadband stations. This method is more advantageous than other classical seismic techniques because it does not depend on earthquakes seismicity and source parameters and since it is a low cost and simple operation method.

It has been theoretically demonstrated that the cross-correlation of the recorded diffuse wavefields, such as ambient seismic noise, can provide an estimate of the empirical Green's function which mostly consists of fundamental Rayleigh waves that travel between the two stations as if they would be generated at one of the stations. These empirical Green's functions provide information of the structure of the crust between the station pairs [23–27]. We applied the cross-correlation technique to records of ambient seismic noise from the microseismic frequency band. The corresponding sources are in the oceans due to gravity wave activity caused by atmospheric perturbations [28–31]. Here we present shear wave velocity models inferred from the Rayleigh wave group velocities inversion obtained from ambient seismic noise cross-correlation. This study represents the first analysis of ambient seismic noise registered in TdF in order to constrain the upper crust beneath this region.

2. Methodology

2.1. Data

In order to study the upper crustal structure we used data recorded at four broadband seismic stations installed in the Argentinian part of TdF: DSPA, ELCA and TRVA belong to the Faculty

of Astronomical and Geophysical Sciences, National University of La Plata (FCAG, UNLP) and to the National Institute of Oceanography and Experimental Geophysics (OGS) and are locally operated by the Astronomical Station of Rio Grande (EARG); USHA belongs to the Comprehensive Nuclear-test-ban Treaty Organization (CTBTO) and its local responsible is the National Institute of Seismic Prevention (INPRES). The stations are equipped with Guralp CMG-3T (0.003–50 Hz), CMG-3TD (0.003–50 Hz), CMG 40T (0.033–50 Hz) and Streckeisen STS-2 (0.01–10 Hz) seismometers and are installed in the Argentinian part of TdF. For our analysis we considered data with 20 and 40 samples per seconds. The station locations are marked by red triangles in the map of Fig. 1.

We considered 12 months of ambient seismic noise continuously registered at all stations. We used the vertical components, since we are interested to extract Rayleigh waves. In order to process the raw seismic data we applied a procedure similar to those described by Bensen et al. [32]: (1) single-station data pre-processing, (2) cross-correlation and stacking, (3) measurement of dispersion and (4) dispersion curves inversion for 1-D shear wave velocity profiles estimation. We used the SAC software [33] to preprocess the data. The single-station data pre-processing was performed according to the following steps: elimination of seismic traces containing spikes or gaps, removal of the instrument response, subtraction of the mean and trend, decimation, band-pass filtering before and after the one-bit temporal normalization and spectral whitening. The data has also been inspected visually to identify and remove data sequences with instrumental irregularities or any other strange noise and data problems. The optimal time-frequency analysis resolution depends mainly on the interstation distances [34]. The upper frequency was set to 0.4 Hz while the lower frequencies were adjusted so that the distance between each pair of stations corresponds, at least to three wavelengths ($\Delta \geq 3\lambda$) [35]. The corresponding values of the lower frequencies range between 0.06 and 0.12 Hz, depending on the interstation distance.

2.2. Cross-correlation and stacking

After data pre-processing, we cross-correlated all possible combinations of station pairs obtaining 6 possible surface wave trajectories. We applied two types of cross-correlation techniques: the classical cross-correlation which is geometrically normalized (CCGN) and the phase cross-correlation (PCC) that is based on analytic signal theory [36]. The main differences between both techniques is that PCC detect signals considering their phase coherence while the CCGN identifies them by the largest sum of amplitude products, thus energy. Because the PCC is not amplitude biased, the pre-processing steps of one-bit temporal normalization and spectral whitening are not necessary as demonstrated by Schimmel et al. [37].

Using long noise recordings improves the signal extraction due to a usually more balanced noise source distribution and constructive summation of coherent signals and destructive cancellation of other less coherent noise. In practice, the long noise recordings are segmented and their cross-correlations are stacked linearly. Moreover, when stacking over long times, the distribution of the ambient seismic sources randomizes and the seismic noise can be considered as a random field. After the cross-correlation, we stacked the traces by applying the linear stack and the time-frequency domain phase-weighted stack (tf-PWS) developed by Schimmel and Gallart [38]. The disadvantage of the linear stack is that weak-amplitude coherent phases may be hidden in larger-amplitude noise. The tf-PWS technique is an extension of the phase-weighted stack (PWS) presented by Schimmel and Paulssen [39] which is a non-linear stack where

each sample of a linear stack is weighted by an amplitude-unbiased coherence measure. The tf-PWS is based on the time-frequency decomposition of each trace using the S-transform [40]. An improvement of the signal to noise ratio and the emergence of Rayleigh waves is observed with both stacking techniques. However, we observed that the application of PCC in combination with the linear stack (tl-PCC) on our data is enough for the extraction of Rayleigh waves. In the following we therefore considered only tl-PCC to extract Rayleigh waves. Fig. 2a shows the linear stack of one year of cross-correlated data (PCC) for all possible station pairs in TdF. In all cases, the emergence of surface waves is observed for negative lag-times. We correlated data from a station located to the north with a station further to the south, which by definition of the cross-correlation used means that waves traveling from north to south are recorded at positive lag time and waves traveling from south to north at negative lag time. The larger energy at negative lag times (Fig. 2a) is therefore due to the dominance of noise sources to the south of TdF. I.e., in the considered frequency band, seismic noise is mostly generated to the south and propagates northward.

Noise source distribution is often not homogeneous and the obtained correlograms are not time-symmetrical as shown in Fig. 2a. In order to average the effects of this distribution, we calculate the so-called symmetrical correlation by averaging the positive and negative lag times (Fig. 2b) [41–43]. This procedure is often used and necessary to improve the signal to noise ratio of the empirical Green's functions. The symmetrical component is used in the following to extract the dispersion curves.

2.3. Rayleigh wave dispersion

In order to measure group velocities of fundamental mode Rayleigh waves retrieved from the obtained ambient seismic noise cross-correlations, we considered the interstation distance that ranges from about 50 km to about 100 km. In general, fundamental mode Rayleigh waves at smaller periods (or higher frequencies) are sensitive to the physical properties of near-surface layers while higher periods (or lower frequencies) are more sensitive to deep structures [44]. Table 1 indicates the frequency range used in this study and consequently the Rayleigh waves retrieved in our analysis are sensible to shallow structures in the upper crust down to about 10 km.

To measure group velocities, we represent the stacked cross-correlograms in the time-frequency domain using the S-transform developed by Stockwell et al. [40]. The Rayleigh wave group arrivals are measured at the maxima in the time-frequency representation. These arrivals in the time-frequency domain are transformed into group velocity considering the interstation distance of each station pair. Fig. 3 shows an example for station pairs DSPA-ELCA and DSPA-TRVA. The dispersion curves obtained through the cross-correlations for all possible pairs of stations are shown in Fig. 4 as a function of period.

In order to test the robustness of the dispersion curves, we analyzed the results considering 10, 20 and 30 days stacks of cross-correlations (Fig. 5) as well as the stack considering different months of the year (Fig. 6). It is seen from Fig. 5 that the dispersion curves converged for most of the periods to stable values after few days. Nevertheless, Fig. 6 shows a variability in the dispersions obtained for different one month data stacks. This variability is likely due to the seasonal distribution of noise sources. It is also seen that this variability mostly affects the measurements below periods $T < 4$ s and $T > 10$ s. In our analysis we use one year data stacks to reduce these seasonal influences through averaging. Figs. 5 and 6 also show the importance of using a large amount of data.

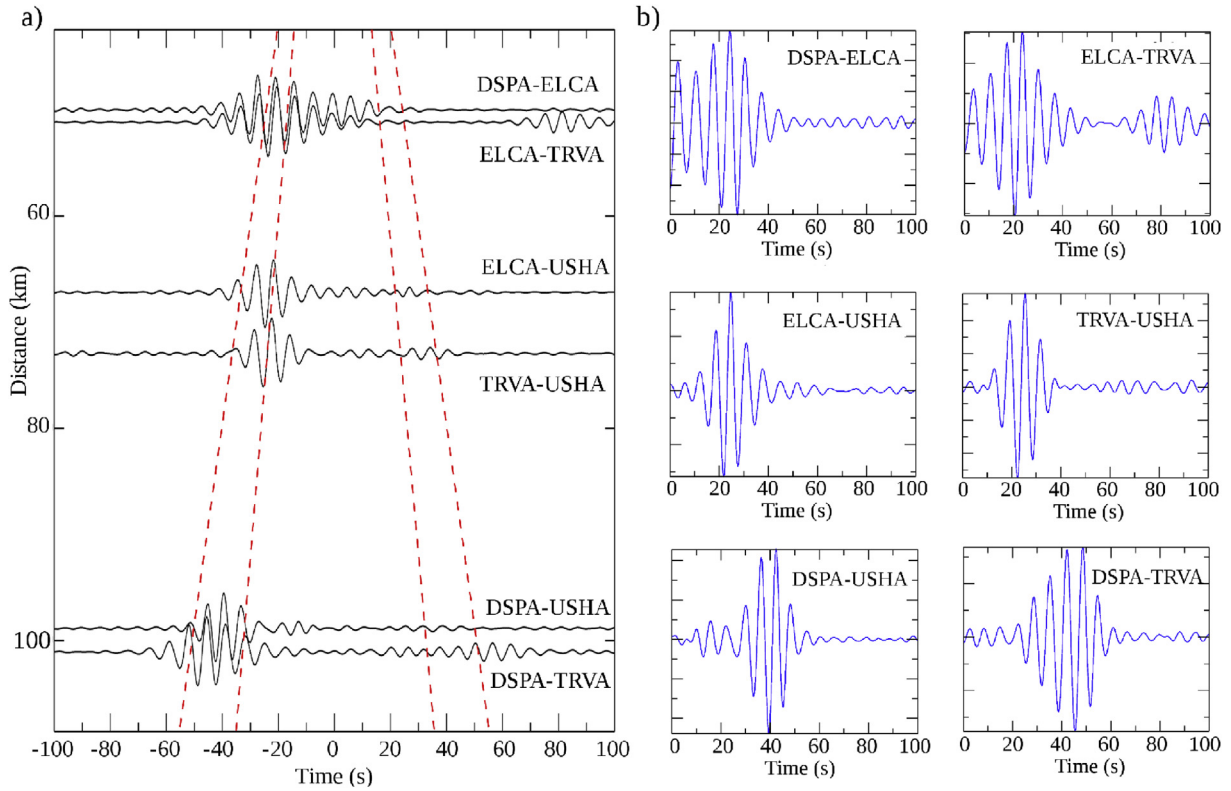


Fig. 2. a) Stacked of cross-correlation (PCC) of ambient seismic noise registered at broadband stations in TdF. Each trace corresponds to the stacked cross-correlations for one single station pair. The red dotted lines indicate the group arrival times for Rayleigh wave velocities of $v = 2$ km/s and $v = 3$ km/s, respectively. The distance between the seismic station pairs is indicated by the vertical axis. b) Symmetrical correlations obtained from the cross-correlation patterns shown in a).

Table 1

Frequencies used in order to measure Rayleigh wave dispersion. The lower and higher frequencies are indicated as f_1 and f_2 respectively.

Cross-correlation	f_1 (Hz)	f_2 (Hz)	Interstation distance (km)
DSPA-ELCA	0.12	0.4	50
TRVA-ELCA	0.12	0.4	50
ELCA-USHA	0.10	0.4	68
TRVA-USHA	0.08	0.4	72
DSPA-USHA	0.06	0.4	98
DSPA-TRVA	0.07	0.4	100

2.4. Estimation of 1-D shear wave velocity models

The dispersion curves shown in Fig. 4 (section 2.3) were inverted to determine 1-D shear wave velocity models beneath the study area. For this purpose, we applied the code SURF96 which belongs to the Computer Programs in Seismology (CPS) package [45]. This algorithm performs a non-linear iterative damped least squares inversion starting from an initial model. The codes inverts observed

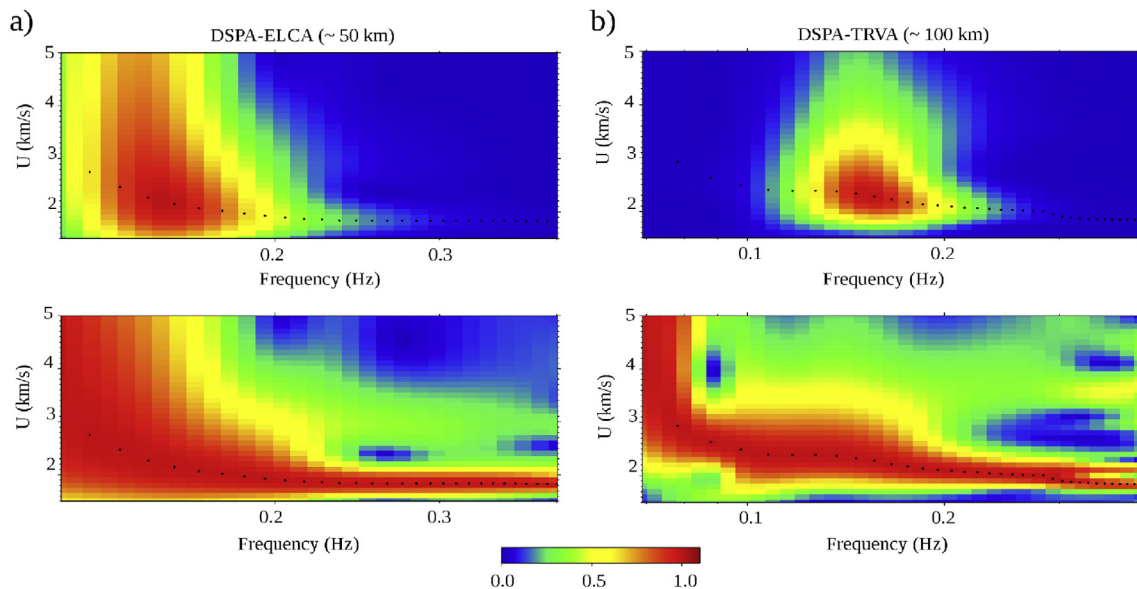


Fig. 3. Group velocities obtained through the cross-correlation of ambient seismic noise recorded at stations a) DSPA and ELCA and b) DSPA and TRVA. We used the linear stack of 1 year data cross-correlated with PCC. To the top we show the overall energy distribution normalized to 1 while to the bottom we show the same data, but where energy has been normalized for each frequency to better track the group arrivals. The frequency axis is logarithmic and the vertical axis indicates the measured group velocity values.

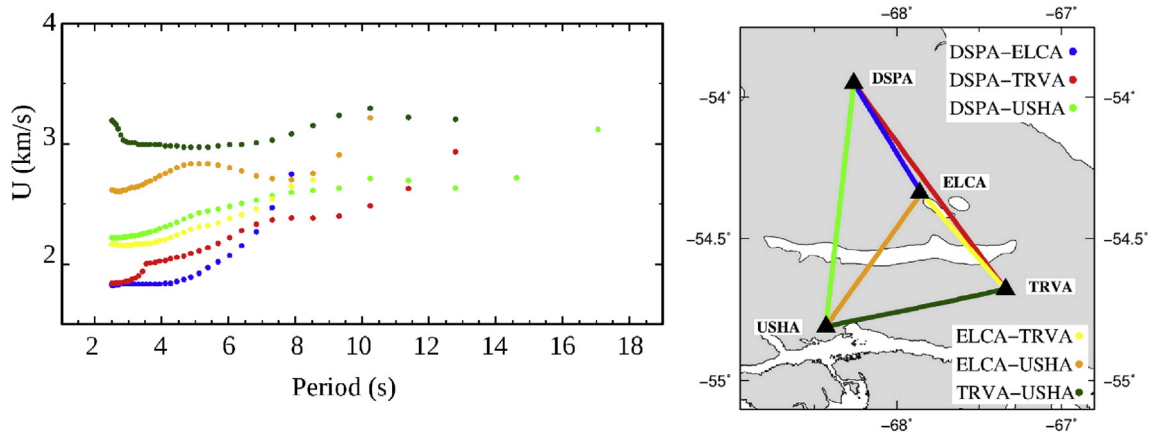


Fig. 4. Rayleigh wave dispersion curves obtained through cross-correlation (PCC) of ambient seismic noise for all possible station combinations. The colors mark the seismic station pairs. Group velocities were measured in the frequency range shown in Table 1. The map at the right shows the corresponding station trajectories.

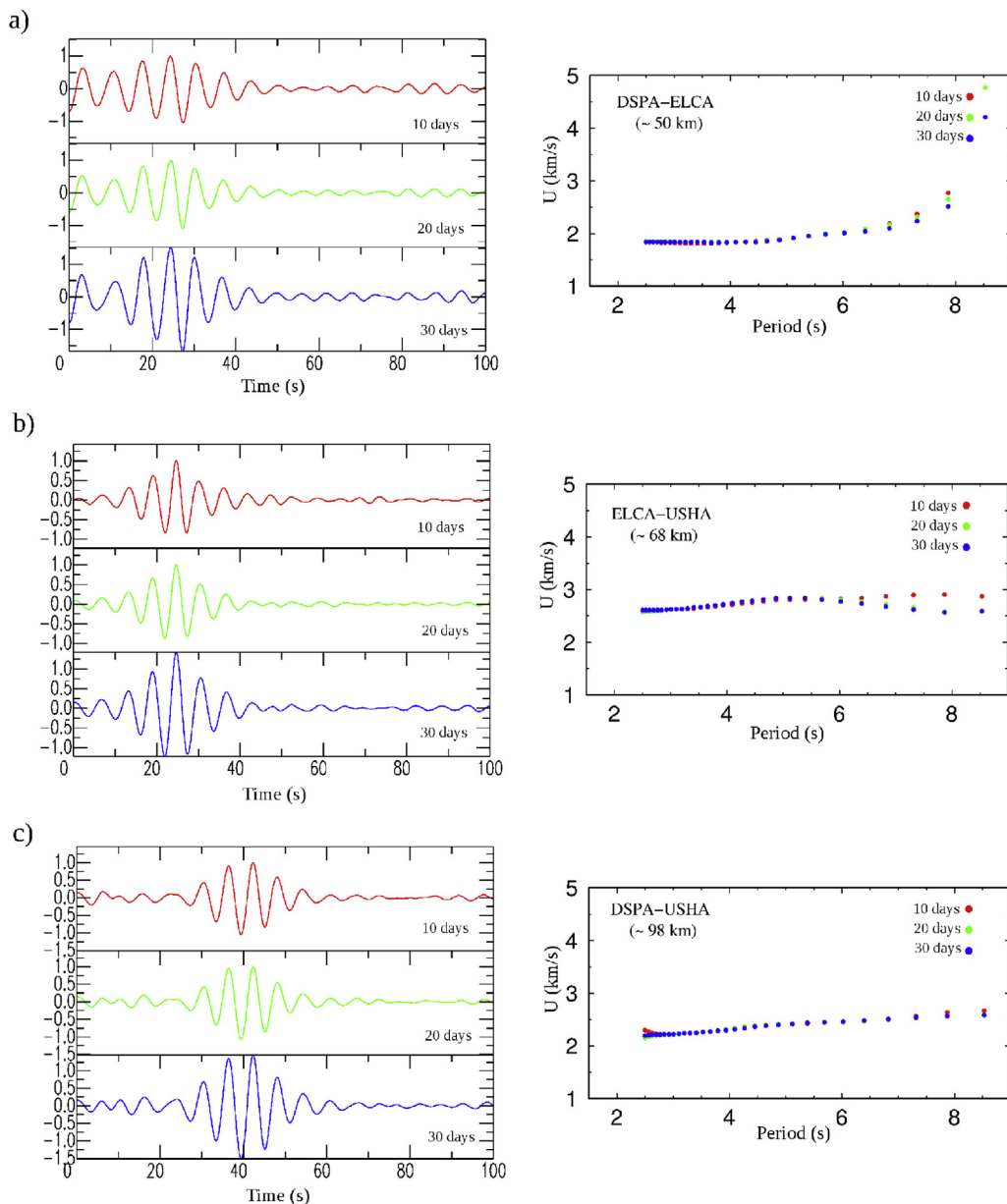


Fig. 5. 10, 20 and 30 days stack of cross-correlation (PCC) of ambient seismic noise registered at station pairs a) DSPA and ELCA, b) ELCA and USHA y c) DSPA and USHA. To the right we show the dispersion curves obtained for each case.

group velocities for plane-layered S-wave structures, and the procedure consists in minimizing velocity differences between adjacent layers considering damping and weighting factors to find the best fitting between the calculated dispersion curves and the observed ones.

The selection of an initial model is a necessary step in the least square inversion. After several tests, we defined three initial models based on the model CRUST 1.0 [46] for the TdF area. It further permits us to see the robustness of the final models with respect to different starting models. The initial models A and B (Table 2) are a parametrization adapted from CRUST 1.0, considering S-wave velocity values higher than the reference model. In both cases, the first 10 km of the crust were divided into layers of 1 km thickness. The third initial model C is an average of the final model obtained as a result of the inversion considering the initial model B and therefore is different for each station pair and dispersion curve. The density (g/cm^3) and P- and S-wave velocity (km/s) values used for the mantle for the three initial models were $\rho = 3.3 \text{ g/cm}^3$, $V_P = 7.99 \text{ km/s}$ and $V_S = 4.44 \text{ km/s}$, respectively, based on CRUST 1.0.

Several preliminary tests were conducted in order to establish the inversion parameters such as the damping, smoothing and weighting factors. Furthermore, the frequency range considered in this study warrants that the observed Rayleigh waves are sensible dominantly to shallow structures in the upper crust. Taking this into account, we fixed velocity and density values for deeper layers and performed the inversion (200 iterations) only for the upper structure of the crust down to 10 km.

Figs. 7 and 8 show the final models which represent the average shear wave velocity structure of the upper crust between each seismic station pair in TdF. It can be observed that the three final models are quite similar for each station pair and that the measured dispersion curves are well fitted by the obtained models with exception of ELCA-USHA (Fig. 8c).

3. Discussion and conclusions

The final models obtained from the inversion of Rayleigh waves dispersion fit reasonably well the measured group velocity

Table 2
Initial models A and B based on model CRUST 1.0.

Thickness (km)	V_P model A (km/s)	V_P model B (km/s)	V_S model A (km/s)	V_S model B (km/s)	$\rho(\text{g/cm}^3)$
1	3.50	3.80	1.52	1.63	2.1
1	3.80	4.00	1.63	1.71	2.2
1	4.20	4.30	2.24	2.30	2.3
1	4.70	4.80	2.51	2.56	2.4
1	4.90	5.00	2.62	2.70	2.5
1	5.20	5.30	2.88	2.94	2.6
1	5.50	5.60	3.07	3.11	2.7
1	5.80	5.90	3.31	3.40	2.7
1	5.90	6.10	3.47	3.50	2.7
1	6.00	6.20	3.50	3.64	2.8
10.5	6.50	6.60	3.74	3.78	2.9
10	7.10	7.10	4.04	4.04	2.9

curves. The best fits were obtained for ELCA-TRVA, DSPA-ELCA, DSPA-TRVA and DSPA-USHA (Figs. 7 and 8) while the models for TRVA-USHA and ELCA-USHA did not explain the data as well as for the other trajectories (Fig. 8). Nevertheless, the misfit of the two latter station pairs is not too large and a clear trend of higher group velocities ($\sim 2.6\text{--}3.3 \text{ km/s}$ for periods between 3 and 9 s) was observed. These station trajectories were more to the south of the island which may indicate a smaller amount of sediments in the south of TdF (Fig. 9). From Fig. 9, we further see at $T = 9 \text{ s}$ a discrepancy between the velocity values measured for paths DSPA-TRVA and DSPA-ELCA + ELCA-TRVA. The variation observed is not expected taking into account the proximity of the trajectories between the stations. This may reflect wave propagation complexities such as multipathing and/or the interference of other signals and noise which do not permit a complete or isolated recovery of the shortest path Rayleigh wave at 9 s of period.

Fig. 10 shows all the final models obtained through the inversion of group velocities measured from cross-correlation of ambient seismic noise in TdF. Due to the short distances between stations (and therefore high frequencies), these models provide information of the most superficial layers of the crust. According to the inversion results, the S-wave velocity ranges between 1.75 and 3.7 km/s

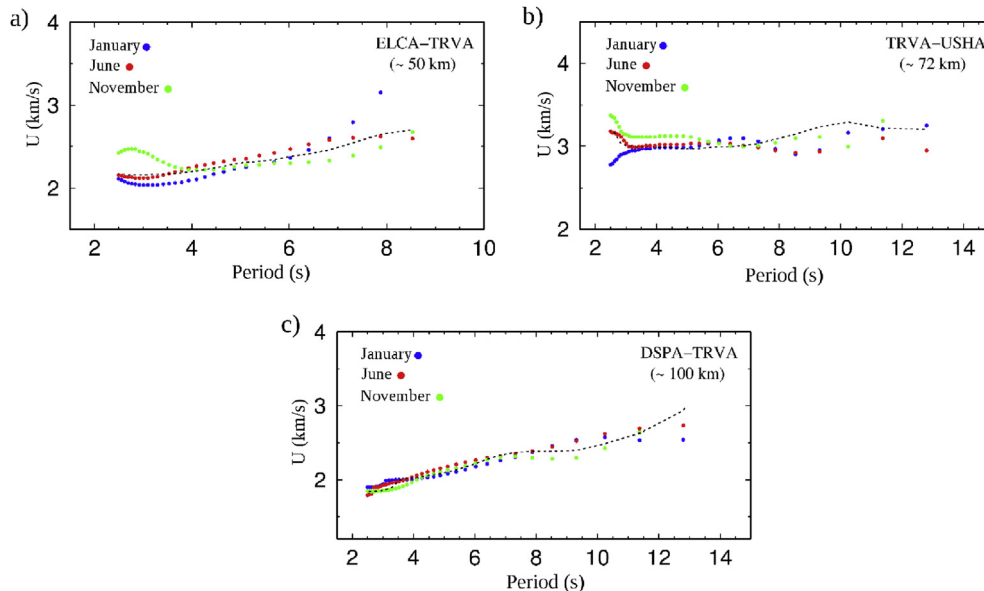


Fig. 6. Dispersion curves measured from the cross-correlation of ambient noise for station pairs a) DSPA and TRVA, b) TRVA and USHA and c) ELCA and TRVA considering different months of the year. The black dotted line is the dispersion curve obtained stacking 1 year of cross-correlation (PCC).

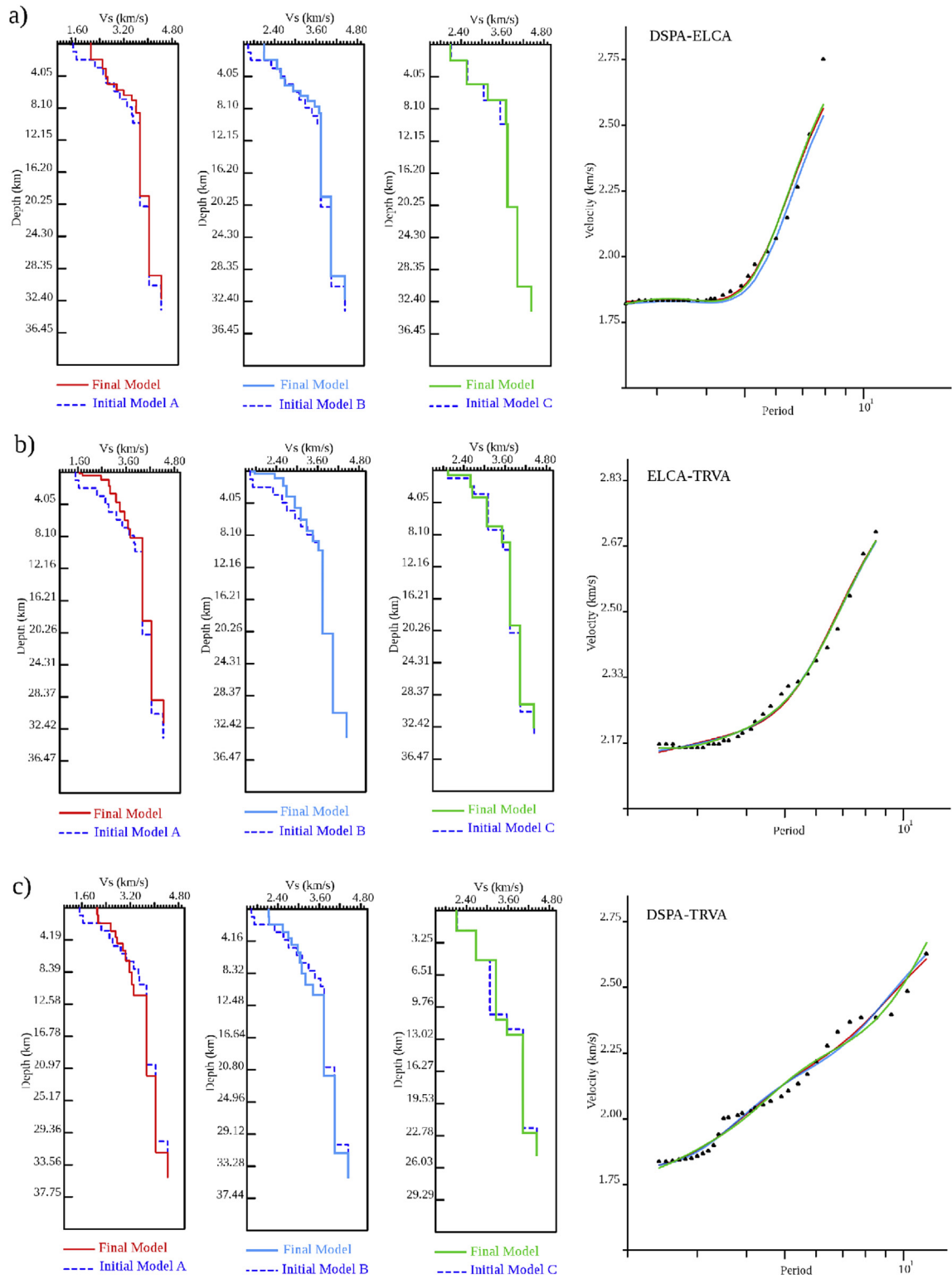


Fig. 7. Inversion results for fundamental mode Rayleigh wave dispersions measured from the cross-correlation of ambient noise for station pairs a) DSPA and ELCA, b) ELCA and TRVA and c) DSPA and TRVA. Final models in red, blue and green correspond to the initial models A, B and C, respectively. Observed group velocities are marked as black triangles (right side), and the best fitting dispersion curves are indicated with colors red, blue and green.

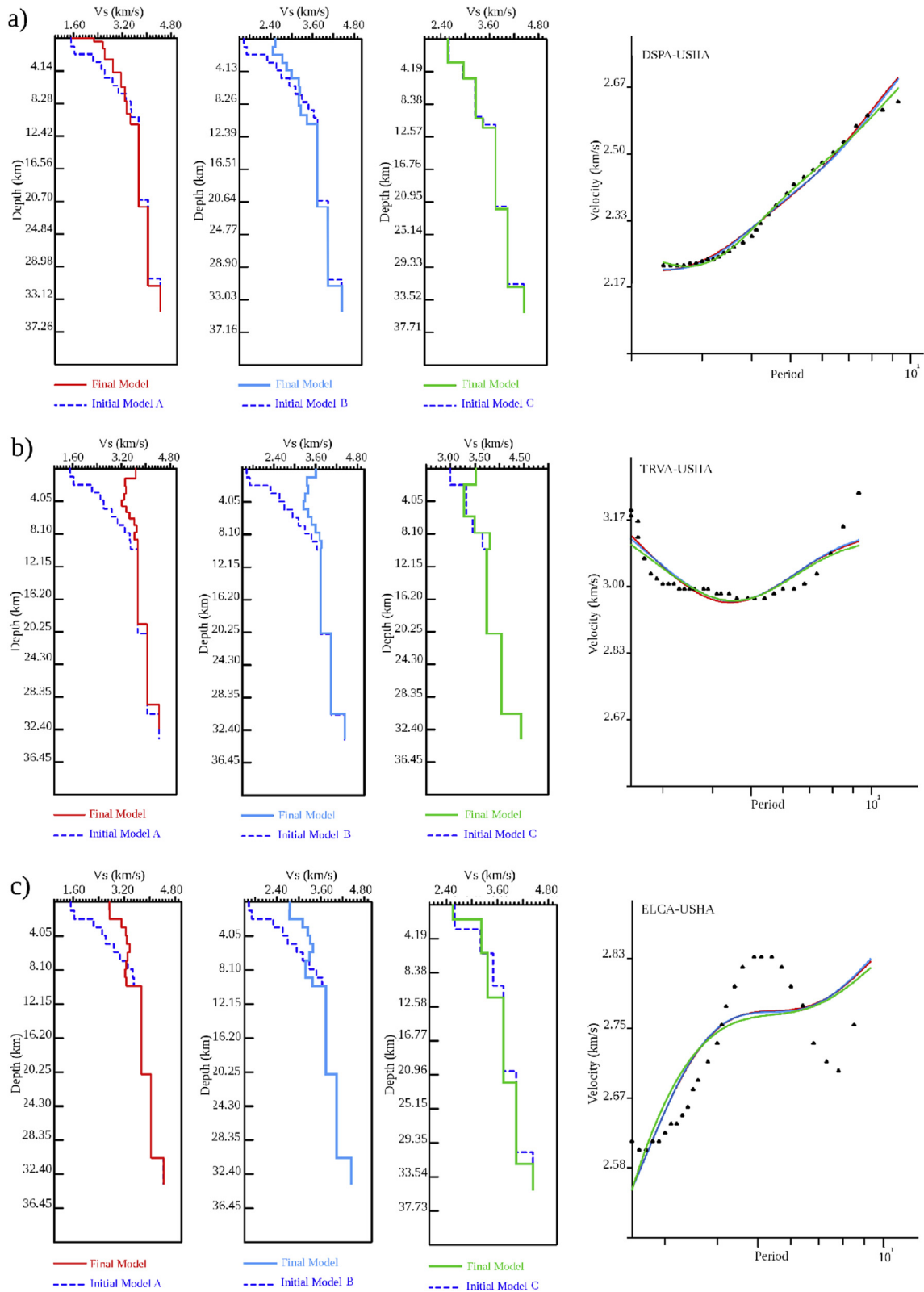


Fig. 8. Inversion results for fundamental mode Rayleigh wave dispersions measured from the cross-correlation of ambient noise for station pairs a) DSPA and USHA, b) TRVA and USHA and c) ELCA and USHA. Final models in red, blue and green corresponds to initial models A, B and C, respectively. Observed group velocities are marked as black triangles (right side), and the best fitting dispersion curves are marked with colors red, blue and green.

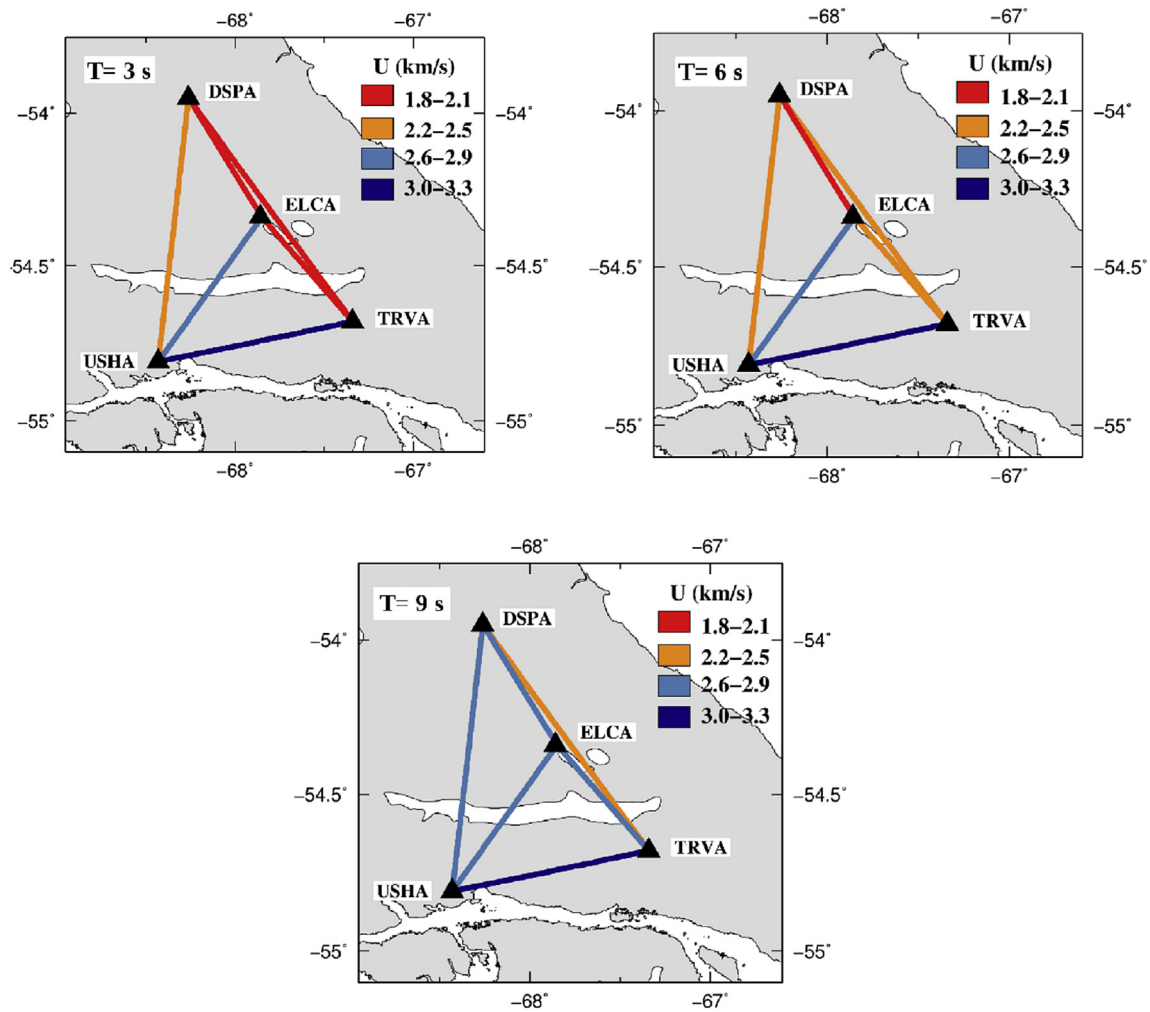


Fig. 9. Group velocities obtained through the cross-correlation (PCC) of ambient seismic noise registered for 1 year. Seismic station positions are marked with black solid triangles. Each line indicates the surface wave trajectory and colors denotes the range of velocities obtained for a period of 3, 6 and 9 s.

in the first 10 km of the crust, depending on the pair of stations considered.

The variability of the obtained models are in accordance with the complex geological and tectonic environment of the area through the presence of several faults and folded structures [2,6,8,12,47,48]. The average upper crustal structure obtained for DSPA-TRVA, DSPA-ELCA and DSPA-USHA is associated with S-wave velocity values ranging from 2.3 to 2.6 km/s for the uppermost layers down to about 2 km depth. We associate this result with the presence of Tertiary and Cretacic sediments [2,8]. On the other hand, the obtained models in the southern part of TdF, reveal that the upper layers of the crust are characterized by higher S-wave velocity values (3.3–3.7 km/s). The southernmost stations, TRVA and USHA, are located in the fold and thrust belt area that involved deformation and cortical thickening of lower Cretacic, Jurassic and Paleozoic basement units [6]. In the case of TRVA-USHA and ELCA-USHA, the fit was not good and final results reveal low velocity zones. This is suggesting that the crust in the south of the island is more complex and the structure cannot be explained with simple 1-D plane-layered models. Besides this, we observed a good correlation between most of the final models and geology, in particular with the superficial-subsuperficial lithology. Younger geological units, composed of less consolidated sediments are associated with

lower S-wave velocities values. To the south, and considering deeper layers, older and more consolidated geological units present higher S-wave velocity values [6].

The inversion procedure was performed considering different inversion parameters, damping and weighting factors as well as different starting models. In all cases, we obtained similar final models which indicate a high degree of robustness. Further, the results presented here are sound in the geological context of TdF indicating a diverse seismic structure of the upper crust beneath the study area.

The study area is classified as moderate to high seismic hazard according to INPRES. A better understanding of the active stress field is therefore crucial, also for risk mitigation. Little is known on the seismic velocity structure of TdF and the here presented models provide new information. A more accurate knowledge on seismic anomalies and seismic structure in general is important, for instance, to permit a better location of earthquakes and consequently higher resolution mapping of fault systems and corresponding stress field. The present study also shows the feasibility of performing ambient noise imaging studies for TdF, based on a higher station density for a more detailed mapping of anomalies and understanding of the tectonics and geology of TdF.

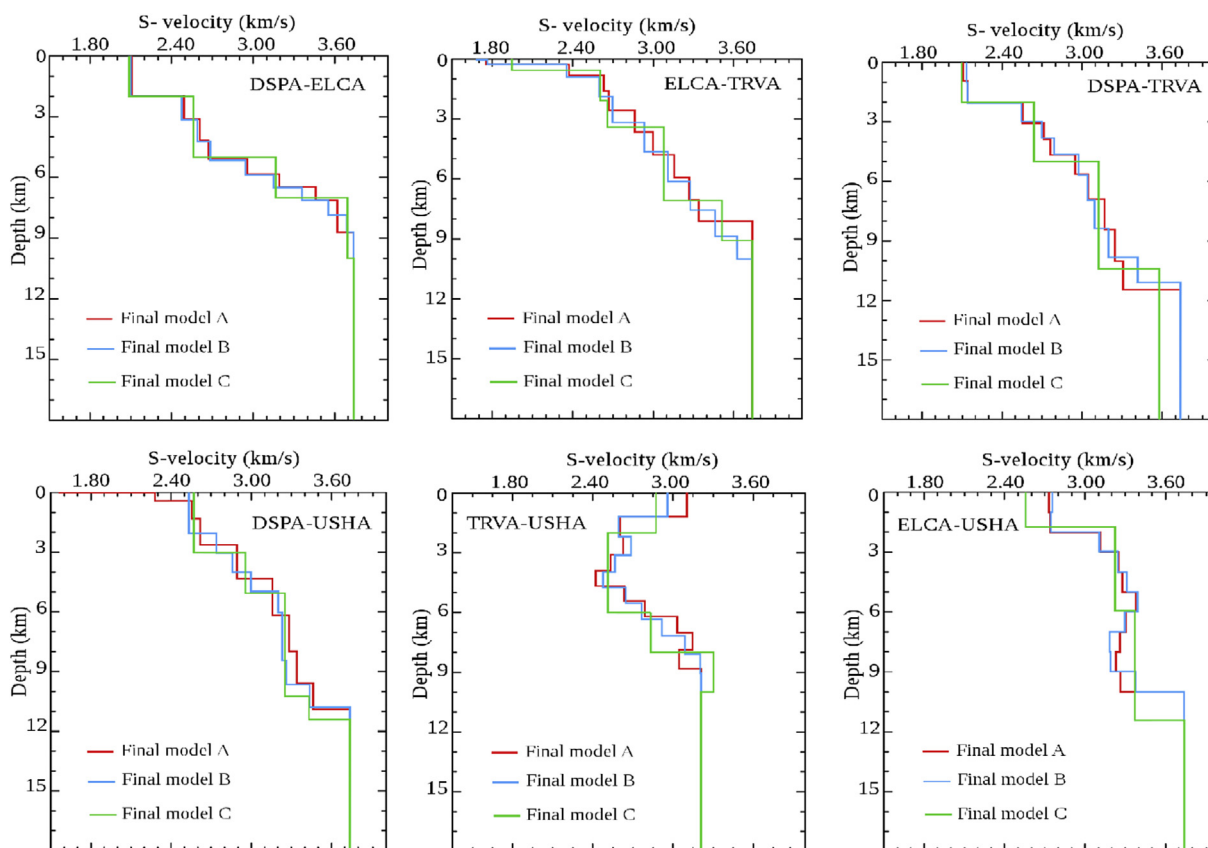


Fig. 10. Results of S-wave velocity models obtained by the inversion of fundamental mode Rayleigh wave dispersion curves. Final models A, B and C are marked in red, blue and green, respectively.

Acknowledgments

The data used in this study was obtained from scientific projects funded by the National Agency for the Promotion of Science and Technology, Argentina (ANPCyT), the National University of La Plata, Argentina (UNLP) and the National Institute of Oceanography and Experimental Geophysics, Italy (OGS). We would like to thank the staff of the Astronomical Station of Rio Grande (EARG) and Marcelo Moreno from the National Institute of Seismic Prevention (INPRES) for operational support in getting data. Furthermore we are grateful to Larminat and Henninger families for allowing us to install the stations DSPA and ELCA respectively and for providing collaboration with EARG. We also would like to thank Alejandro Tassone for his helpful comments on the geology, and Robert Herrmann for providing the CPS package and for his valuable suggestions with the inversion process. We acknowledge the editor for handling the manuscript and referees for providing us with constructive reviews.

References

- [1] A.M. Pelayo, D.A. Wiens, Seismotectonics and relative plate motions in the Scotia Sea region, *J. Geophys. Res. Solid Earth* 94 (1989) 7293–7320, <https://doi.org/10.1029/JB094iB06p07293>.
- [2] E.B. Olivero, D.R. Martinioni, A review of the geology of the Argentinian Fuegian Andes, *J. S. Am. Earth Sci.* 14 (2001) 175–188, [https://doi.org/10.1016/S0895-9811\(01\)00016-5](https://doi.org/10.1016/S0895-9811(01)00016-5).
- [3] R.H. Fuenzalida, *Geological Correlation Between the Patagonian Andes and the Antarctic Peninsula and Some Tectonic Implications*, Master thesis, Stanford University, 1972, p. 75.
- [4] I.W.D. Dalziel, R.L. Brown, Tectonic denudation of the Darwin metamorphic core complex in the Andes of Tierra del Fuego, southernmost Chile: implications for Cordilleran orogenesis, *Geology* 17 (1989) 699–703, [https://doi.org/10.1130/0091-7613\(1989\)017<0699:TDOTDM>2.3.CO;2](https://doi.org/10.1130/0091-7613(1989)017<0699:TDOTDM>2.3.CO;2).
- [5] L. Mendoza, A. Richter, M. Fritsche, J.L. Hormaechea, R. Perdomo, R. Dietrich, Block modeling of crustal deformation in Tierra del Fuego from GNSS velocities, *Tectonophysics* 651–652 (2015) 58–65, <https://doi.org/10.1016/j.tecto.2015.03.013>.
- [6] M. Menichetti, E. Lodolo, A. Tassone, Structural geology of the Fuegian Andes and Magallanes fold-and-thrust belt—Tierra del Fuego Island, *Geol. Acta* 6 (2008) 19–42.
- [7] I.W.D. Dalziel, R.H. Dott Jr., R.D. Winn Jr., R.L. Bruhn, Tectonic relations of south Georgia island to the southernmost Andes, *Geol. Soc. Am. Bull.* 86 (1975) 1034–1040, [https://doi.org/10.1130/0016-7606\(1975\)86<1034:TROSGI>2.0.CO;2](https://doi.org/10.1130/0016-7606(1975)86<1034:TROSGI>2.0.CO;2).
- [8] A. Tassone, H. Lippai, E. Lodolo, M. Menichetti, A. Comba, J.L. Hormaechea, J.F. Vilas, A geological and geophysical crustal section across the Magallanes-Fagnano fault in Tierra del Fuego and associated asymmetric basins formation, *J. S. Am. Earth Sci.* 19 (2005) 99–109, <https://doi.org/10.1016/j.jsames.2004.12.003>.
- [9] R. Caminos, F. Nullo, Descripción geológica de la Hoja 67e. Isla de Los Estados, *Boletín del Servicio Geológico Nacional (Argentina)* 175 (1979) 1–175.
- [10] R. Caminos, M.A. Hall, O. Lapido, A. Lizuaín, R. Page, V. Ramos, Reconocimiento geológico de los Andes Fueguinos, territorio Nacional de Tierra del Fuego, IX Congreso Geológico Argentino, Buenos Aires Actas III (1981) 759–786.
- [11] M.C. Ghiglione, *Estructura y evolución tectónica del cretácico terciario de la Costa Atlántica de Tierra del Fuego*, Tesis Doctoral, Universidad de Buenos Aires, 2003, p. 197.
- [12] E. Lodolo, M. Menichetti, R. Bartole, Z. Ben-Avraham, A. Tassone, H. Lippai, Magallanes-Fagnano continental transform fault (Tierra del Fuego, southernmost South America), *Tectonics* 22 (2003) 1076, <https://doi.org/10.1029/2003TC001500>.
- [13] K.A. Klepeis, The Magallanes and Deseado fault zones: major segments of the South American-Scotia transform plate boundary in southernmost South America, Tierra del Fuego, *J. Geophys. Res.* 99 (1994) 22001–22014, <https://doi.org/10.1029/94JB01749>.
- [14] J.M. Febrer, M.P. Plasencia, N. Sabbione, Local And Regional Seismicity from Ushuaia Broadband Station Observations (Tierra del Fuego), *Terra Antarctica* 8 (2000) 35–40.
- [15] N.C. Sabbione, G. Connon, J.L. Hormaechea, M.L. Rosa, Estudio de sismicidad en la provincia de Tierra del Fuego, Argentina, *Geoacta* 32 (2007) 41–50.

- [16] C. Buffoni, Estudio de sismicidad en la Isla de Tierra del Fuego, Bachelor thesis, Faculty of Astronomical and Geophysical Sciences, National University of La Plata, 2008.
- [17] C. Buffoni, N.C. Sabbione, G. Connon, J.L. Hormaechea, Localización de hipocentros y determinación de su magnitud en Tierra del Fuego y zonas aledañas, *Geoacta* 34 (2009) 75–85.
- [18] C. Lomnitz, Major earthquakes and tsunamis in Chile, *Geologische Rundschau* 59 (1970) 938–960, <https://doi.org/10.1007/BF02042278>.
- [19] E. Jaschek, N. Sabbione, P. Sierra, Reubicación de sismos localizados en territorio argentino (1920–1963), Vol. XI of *Geofísica*, Publicaciones Observatorio de la Universidad Nacional de La Plata, 1982.
- [20] W.J. Ludwig, J.I. Ewing, M. Ewing, Seismic refraction measurements in the Magellan Straits, *J. Geophys. Res.* 70 (1965) 1855–1876, <https://doi.org/10.1029/JZ070i008p01855>.
- [21] S.D. Robertson Maurice, D.A. Wiens, K.D. Koper, E. Vera, Crustal and upper mantle structure of southernmost South America inferred from regional waveform inversion, *J. Geophys. Res.* 108 (B1) (2003) 2038, <https://doi.org/10.1029/2002JB001828>.
- [22] J.F. Lawrence, D.A. Wiens, Combined receiver-function and surface wave phase-velocity inversion using a niching genetic algorithm; application to Patagonia, *Bull. Seismol. Soc. Am.* 94 (2004) 977–987, <https://doi.org/10.1785/0120030172>.
- [23] R.L. Weaver, O.I. Lobkis, On the emergence of the Green's function in the correlations of a diffuse field, *J. Acoust. Soc. Am.* 110 (2001) 3011–3017, <https://doi.org/10.1121/1.1417528>.
- [24] A. Derode, E. Larose, M. Tanter, J. de Rosny, A. Tourin, M. Campillo, M. Fink, Recovering the Green's function from field-field correlations in an open scattering medium (L), *J. Acoust. Soc. Am.* 113 (2003) 2973–2976, <https://doi.org/10.1121/1.1570436>.
- [25] R. Snieder, Extracting the Green's function from the correlation of coda waves: a derivation based on stationary phase, *Phys. Rev. E* 69 (046610) (2004) 1–8, <https://doi.org/10.1103/PhysRevE.69.046610>.
- [26] K. Wapenaar, J. Thorbecke, D. Draganov, Relations between reflection and transmission responses of three-dimensional inhomogeneous media, *Geophys. J. Int.* 156 (2) (2004) 179–194, <https://doi.org/10.1111/j.1365-246X.2003.02152.x>.
- [27] E. Larose, A. Khan, Y. Nakamura, M. Campillo, Lunar subsurface investigated from correlation of seismic noise, *Geophys. Res. Lett.* 32 (16) (2005) L16201, <https://doi.org/10.1029/2005GL023518>.
- [28] A. Friedrich, F. Krueger, K. Klinge, Ocean-generated microseismic noise located with the Gräfenberg array, *J. Seismol.* 2 (1) (1998) 47–64.
- [29] P. Lognonné, E. Clévéde, H. Kanamori, Computation of seismograms and atmospheric oscillations by normal-mode summation for a spherical earth model with realistic atmosphere, *Geophys. J. Int.* 135 (2) (1998) 388–406, <https://doi.org/10.1046/j.1365-246X.1998.00665.x>.
- [30] T. Tanimoto, Excitation of normal modes by atmospheric turbulence: source of long-period seismic noise, *Geophys. J. Int.* 136 (1999) 395–402, <https://doi.org/10.1046/j.1365-246X.1999.00763.x>.
- [31] E. Stutzmann, M. Schimmel, G. Patau, A. Maggi, Global climate imprint on seismic noise, *Geochem. Geophys. Geosystems* 10 (11) (2009), <https://doi.org/10.1029/2009GC002619>.
- [32] G.D. Bensen, M.H. Ritzwoller, M.P. Barmin, A.L. Levshin, F.C. Lin, M.P. Moschetti, N.M. Shapiro, Y. Yang, Processing seismic ambient noise data to obtain reliable broad-band surface wave dispersion measurements, *Geophys. J. Int.* 169 (3) (2007) 1239–1260, <https://doi.org/10.1111/j.1365-246X.2007.03374.x>.
- [33] P. Goldstein, A. Snoko, SAC Availability for the IRIS Community, Vol VII, No 1, Incorporated Institutions for Seismology Data Management Center Electronic Newsletter, 2005. <http://ds.iris.edu/ds/newsletter/vol7/no1/sac-availability-for-the-iriscommunity/>.
- [34] N.M. Shapiro, S.K. Singh, Short note: a systematic error in estimating surface-wave group-velocity dispersion curve and a procedure for its correlation, *Bull. Seismol. Soc. Am.* 89 (4) (1999) 1138–1142.
- [35] G.D. Bensen, M.H. Ritzwoller, N.M. Shapiro, Broadband ambient noise surface wave tomography across the United States, *J. Geophys. Res.* 113 (2008) B05306, <https://doi.org/10.1029/2007JB005248>.
- [36] M. Schimmel, Phase cross-correlations: design, comparisons and applications, *Bull. Seismol. Soc. Am.* 89 (1999) 1366–1378.
- [37] M. Schimmel, E. Stutzmann, J. Gallart, Using instantaneous phase coherence for signal extraction from ambient noise data at a local to a global scale, *Geophys. J. Int.* 184 (2011) 494–506, <https://doi.org/10.1111/j.1365-246X.2010.04861.x>.
- [38] M. Schimmel, J. Gallart, Frequency-dependent phase coherence for noise suppression in seismic array data, *J. Geophys. Res.* 112 (2007) B04303, <https://doi.org/10.1029/2006JB004680>.
- [39] M. Schimmel, H. Paulssen, Noise reduction and detection of weak, coherent signals through phase weighted stacks, *Geophys. J. Int.* 130 (1997) 497–505, <https://doi.org/10.1111/j.1365-246X.1997.tb05664.x>.
- [40] R.G. Stockwell, L. Mansinha, R.P. Lowe, Localization of the complex spectrum: the S transform, *IEEE Trans. Signal Process.* 44 (4) (1996) 998–1001, <https://doi.org/10.1109/78.492555>.
- [41] L. Stehly, M. Campillo, N.M. Shapiro, A study of the seismic noise from its long-range correlation properties, *J. Geophys. Res.* 111 (2006) B10306, <https://doi.org/10.1029/2005JB004237>.
- [42] Y. Yang, M.H. Ritzwoller, A.L. Levshin, N.M. Shapiro, Ambient noise Rayleigh wave tomography across Europe, *Geophys. J. Int.* 168 (2007) 259–274, <https://doi.org/10.1111/j.1365-246X.2006.03203.x>.
- [43] H. Yao, R.D. Van Der Hilst, Analysis of ambient noise energy distribution and phase velocity bias in ambient noise tomography, with application to SE Tibet, *Geophys. J. Int.* 179 (2009) 1113–1132, <https://doi.org/10.1111/j.1365-246X.2009.04329.x>.
- [44] S. Stein, M. Wysession, *An introduction to seismology, earthquakes, and earth structure*, Blackwell Pub, Malden, MA, 2003.
- [45] R.B. Herrmann, Computer programs in seismology: an evolving tool for instruction and research, *Seism. Res. Lett.* 84 (2013) 1081–1088, <https://doi.org/10.1785/0220110096>.
- [46] G. Laske, G. Masters, Z. Ma, M. Pasyanos, Update on CRUST1.0—a 1-degree global model of Earth's crust, *Geophys. Res. Abstr.* 15 (2013) EGU2013–EGU2658.
- [47] E. Lodolo, M. Menichetti, C. Zanolla, H.F. Lippai, J.L. Hormaechea, A. Tassone, Gravity map of the Isla Grande de Tierra del Fuego, and morphology of Lago Fagnano, *Geol. Acta* 5 (4) (2007) 0307–0314.
- [48] P.E. Kraemer, Orogenic shortening and the origin of the Patagonian orocline (56 S. Lat), *J. S. Am Earth Sci.* 15 (7) (2003) 731–748, [https://doi.org/10.1016/S0895-9811\(02\)00132-3](https://doi.org/10.1016/S0895-9811(02)00132-3).



Carolina Buffoni received a Ph.D in Geophysics from National University of La Plata, Argentina (2017). Her research focused on estimate the crustal structure beneath Great Island of Tierra del Fuego, Argentina, from receiver function and ambient seismic noise analyses.